Research Article

Vaddepalli Pradeep, Pankaj Kumar, Robert Cep, Rajasri Reddy, Ajay Kumar*, and Ashish Kumar Srivastava

Optimization of abrasive water jet machining parameters for basalt fiber/SiO_2 nanofiller reinforced composites

https://doi.org/10.1515/ntrev-2025-0239
received July 29, 2025; accepted October 6, 2025

Abstract: To minimize machining-induced delamination and surface roughness during abrasive water jet machining (AWJM) of basalt-fiber/silica dioxide (SiO_2)-nanofiller epoxy laminates and to define process windows for high-quality holes/slots. Laminates were fabricated from basalt fiber mats (0°/90°) in an epoxy matrix containing 2–8 wt% SiO_2 nanoparticles. AWJM trials systematically varied cutting speed, abrasive flow rate, and stand-off distance (SOD), with jet pressure examined to interpret damage mechanisms. Responses included entry/exit delamination factor (image-based, equivalent-diameter metric) and surface roughness (R_a), complemented by scanning electron microscopy (SEM) of cut edges. A response surface methodology (RSM) with multi-response desirability optimization was used to develop predictive models and identify optimal settings. Lower cutting speeds, moderate abrasive flow, and higher SOD consistently reduced delamination and improved surface finish; SEM revealed that higher jet pressure suppressed matrix washout and fiber pull-out, whereas low pressure increased surface defects. The RSM models showed strong predictive agreement with validation experiments, enabling contour maps and trade-off curves for concurrent delamination–roughness control. The study provides experimentally validated guidelines for precise parameter control in AWJM of basalt/SiO_2 laminates, supporting low-damage, assembly-grade machining of composite components. The resulting process windows are directly applicable to aerospace (*e.g.*, brackets, panels, fittings), automotive (lightweight structures), and construction where surface integrity and structural reliability are critical.

Keywords: water jet machining, basalt fiber, SiO_2 nanofillers, composite materials, material removal rate, surface roughness

1 Introduction

The machining of composite materials, particularly fiber-reinforced composites, presents significant challenges due to their heterogeneous nature [1–3]. Conventional machining processes such as milling and drilling often cause defects like delamination, fiber pull-out, matrix cracking, and excessive tool wear, which degrade the material's mechanical performance [4]. While Kovačević *et al.* [5] synthesized the abrasive water jet machining (AWJM) state-of-the-art, linking jet hydrodynamics and key parameters (pressure, stand-off distance [SOD], traverse speed, abrasive size/flow) to removal mechanisms and outcomes, including trade-offs from nozzle wear and piercing strategies. Dahiya *et al.* [6] reviewed AWJM of polymer–matrix composites, synthesizing jet hydrodynamics, erosion mechanisms, and the influence of pressure, stand-off, traverse speed, and abrasive type/flow on kerf taper, roughness, and delamination. They compare AWJM with conventional drilling, highlight entry–exit damage asymmetry, submerged cutting, and multi-pass strategies, and survey modeling/optimization methods. The article identifies

* **Corresponding author: Ajay Kumar**, Department of Mechanical Engineering, School of Core Engineering, Faculty of Science, Technology & Architecture, Manipal University, Jaipur, India, e-mail: ajay.kumar30886@gmail.com, ajay.kumar1@jaipur.manipal.edu
Vaddepalli Pradeep: Department of Mechanical Engineering, SR University, Warangal, India; Department of Mechanical Engineering, Kakatiya Institute of Technology and Science, Warangal, India, e-mail: pradeepkits413@gmail.com
Pankaj Kumar: Department of Mechanical Engineering, SR University, Warangal, India, e-mail: pikupankaj82@gmail.com
Robert Cep: Department of Machining, Assembly and Engineering Metrology, Faculty of Mechanical Engineering, VSB-Technical University of Ostrava, 70800, Ostrava, Czech Republic, e-mail: robert.cep@vsb.cz
Rajasri Reddy: Department of Humanities and Science, Sumathi Reddy Institute of Technology for Women, Warangal, India, e-mail: rajasrii331@gmail.com
Ashish Kumar Srivastava: Department of Mechanical Engineering, Muzaffarpur Institute of Technology, Muzaffarpur, 842003, Bihar, India, e-mail: ashish7185@gmail.com
ORCID: Ajay Kumar 0000-0001-7306-1902

research gaps in precision control, sensing, nozzle wear, and abrasive recycling.

Anu Kuttan *et al.* [7] present a state-of-the-art review of AWJM, organizing process techniques (pure/abrasive jet, drilling/milling, submerged) and parameters (pressure, traverse speed, SOD, abrasive type/size/flow, nozzle geometry) against outcomes such as kerf taper, roughness, and delamination. They explored modeling/optimization and highlight open challenges-nozzle wear, abrasive reuse/sustainability, real-time sensing and control, predictive kerf models, and micromachining precision-and-propose research directions toward closed-loop, greener, and higher-accuracy AWJM. Biswas *et al.* [8] studied erosive wear of SiC-filled glass–polyester composites using a combined experiment and finite-element (FE) approach. A Taguchi L27 design varied impact velocity (43–65 m/s), SiC content (0–20 wt%), impingement angle (30°–90°), SOD (65–85 mm), and erodent size (250–450 μm); analysis of variance (ANOVA) identified impact velocity and angle as primary drivers of erosion. The FE model (multi-particle, 3D) replicated trends and revealed damage progression. SEM confirmed micro-cutting/micro-ploughing; SiC improved resistance up to an optimal loading.

Gawade *et al.* [9] investigated how water pressure and SOD affect kerf taper angle when AWJM cutting an epoxy–glass fiber laminate, keeping other parameters constant. They found taper increases with SOD due to jet divergence, whereas higher pressure reduces taper; the minimum taper angle of 0.34° occurred at 32 ksi (~221 MPa) with SOD at 2 mm. They also reported the width of the cut significantly influences taper, providing practical guidance for minimizing kerf errors in glass-fiber-reinforced polymer (GFRP) AWJM. Vigneshwaran *et al.* [10] present a concise review of AWJM for fiber-reinforced composites, organizing how key parameters like jet pressure, traverse speed, SOD, abrasive size/flow, and nozzle geometry govern responses such as kerf taper, surface roughness, and delamination, with emphasis on entry/exit damage asymmetry. They summarize process variants (submerged cutting, multi-pass, oscillation) and model-based optimization, offering practical guidance on parameter windows for low-damage cutting of composites. Mm *et al.* [11] experimentally minimized kerf taper and delamination in AWJM of hybrid FRP. Using RSM, they showed that the kerf ratio is governed chiefly by SOD and traverse rate, while entry/exit delamination depends on abrasive flow rate, traverse rate, and hydraulic pressure. Raising the jet's kinetic energy (higher pressure/abrasive feed) at lower cutting speed produced the lowest kerf taper and delamination; model–experiment agreement was within 5%, yielding practical parameter windows for low-damage cutting.

Karakurt *et al.* [12] experimentally analyzed kerf angle (taper) in AWJ cutting of granite, relating it to key parameters: water pressure, traverse speed, SOD, abrasive flow rate, and grit size. They showed kerf angle increases with larger SOD and faster traverse and decreases with higher pressure and adequately high abrasive feed; grit size had a secondary, interaction-dependent effect. The authors provided empirical prediction models and recommended high pressure, low traverse speed, and small SOD to minimize taper in stone machining. Rajesh *et al.* [13] studied AWJM of a Ti metal–interleaved basalt–flax fiber metal laminate (FML), varying water-jet pressure, traverse speed, and abrasive flow to evaluate surface roughness, kerf ratio/taper, and edge damage. They found that increasing jet pressure improves surface finish and reduces kerf ratio, while a moderate traverse speed (~30 mm/min) yields near-defect-free holes; SEM observations corroborated cleaner edges under these conditions. The article provides practical parameter windows for machining hybrid Ti/basalt-flax FMLs used in lightweight structures. Singh and Thakur [14] studied AWJM of multi-walled carbon nanotube (MWCNT)-embedded GFRP laminates, varying jet pressure, traverse rate, SOD, and MWCNT content to evaluate kerf taper, surface roughness (R_a), material removal rate (MRR), and entry/exit delamination factors using a Taguchi/ANOVA framework. They report that adding MWCNTs improves overall machinability, enabling lower delamination and better surface quality under optimized parameter sets, and provides parameter–response models useful for selecting AWJM windows for nano-modified GFRP parts.

Vijayabhaskar *et al.* [15] studied AWJM of hybrid basalt–glass/epoxy laminates filled with nano-SiC (0–1 wt%), using an RSM D-optimal design (24 runs) that varied jet pressure (200–600 MPa), SOD (3–15 mm), traverse speed (2–10 mm min^{-1}), and filler content; responses were surface roughness (R_a) and MRR, with optimization *via* a swarm-intelligence (artificial bee colony) algorithm. They report that higher pressure and lower speed generally lower R_a and raise MRR, with SOD showing a non-linear quality/throughput trade-off; 1 wt% nano-SiC also improved laminate mechanical properties and aided machinability. The joint RSM–SI optimization predicted a best setting near pressure ≈553 MPa, speed ≈9.72 mm min^{-1}, SOD ≈ 5.78 mm for favorable R_a–MRR performance. Doreswamy *et al.* [16] examined AWJM of a graphite/glass/epoxy hybrid laminate, using a designed set of cuts that varied water pressure, traverse speed, SOD, abrasive flow, and grit size. Responses – kerf taper, surface roughness, MRR, and edge damage/delamination – were analyzed *via* ANOVA/regression. They found pressure and abrasive flow chiefly govern MRR and taper (higher pressure, adequate abrasive → lower taper), while traverse speed and SOD primarily affect roughness and delamination (higher values worsen quality).

Recommended windows were high pressure, low-to-moderate traverse, small SOD, with microscopy showing reduced fiber pull-out at higher jet energy. Armağan and Arici [17] evaluated AWJM of glass/vinyl-ester laminates using a Taguchi design varying SOD, abrasive mass flow rate (AMFR), traverse speed, water pressure, and laminate thickness (three levels each). Responses were top kerf width (TKW) and surface roughness (R_a), analyzed *via* ANOVA and linear regression; SOD emerged as the most influential factor on TKW, while pressure/AMFR and speed strongly affected R_a. The study recommends high pressure, low traverse speed, and small SOD to minimize kerf and improve finish, with thickness increasing TKW.

Thakur and Singh [18] studied AWJM of MWCNT-doped epoxy/carbon laminates using a Taguchi design with factors MWCNT wt%, jet pressure, traverse rate, and SOD; responses were R_a, kerf taper, MRR, and entry/exit delamination factors. ANOVA and grey relational analysis showed MWCNT content and jet pressure most strongly influence the combined performance. The optimized setting reduced R_a (−25.31%), kerf taper (−23.94%), entry DF (−26.08%), exit DF (−26.16%), and increased MRR (+4.25%) vs the baseline, with model–experiment agreement reported. Mm *et al.* [19] minimized kerf taper and delamination in AWJM of hybrid FRP using RSM/ANOVA. They found SOD and traverse speed chiefly control kerf taper, while abrasive flow rate, traverse speed, and pressure govern entry/exit delamination. Operating at higher pressure with adequate abrasive feed, low traverse, and small SOD delivered the lowest taper and damage. Their predictive models matched experiments within 5%, offering practical parameter windows for low-damage cutting. Shanmugam *et al.* [20] analyzed delamination mechanisms in AWJM of graphite/epoxy and showed that (i) shock-wave impact during initial jet entry creates micro-crack tips and (ii) subsequent water penetration causes water-wedging and abrasive embedment, driving delamination growth. They developed a semi-analytical, energy-based model to predict the maximum delamination length, which matched experiments and offers a process-planning guide for minimizing defects in composite cutting. This work is widely cited as a mechanistic baseline for AWJ parameter selection in laminates.

Across three recent studies, drilling quality in aerospace laminates is shown to depend jointly on cutting parameters, tool design, and laminate architecture. In glass/epoxy, Yalçın *et al.* [21] used a Taguchi L16 design with a newly designed drill and reported that feed rate is the dominant driver of thrust force, smaller diameters generally lower forces, and there is a practical trade-off: mid-speed/low-feed settings minimize thrust, whereas low speed with a medium feed can minimize delamination. In carbon-fiber-reinforced polymer (CFRP), Bolat *et al.* [22] (Taguchi L18) found that a 120° twist drill outperformed a brad-point and larger point-angle tools; higher cutting speed and lower feed reduced surface roughness and delamination, while small diameters increased thrust-reinforcing that geometry and feed control hole integrity. Complementing the process/tool view, Bilal *et al.* [23] showed that the laminate itself co-governs damage: stacking sequence and fiber orientation significantly modulate delamination severity (small holes and higher ply counts being more susceptible), with larger off-axis orientations tending to mitigate damage. Collectively, these works indicate that suppressing drilling-induced delamination in CFRP/GFRP requires co-optimization of feed–speed–geometry with laminate lay-up, motivating integrated design-of-experiments and data-driven maps for selecting process windows.

Conventional drilling of basalt-fiber laminates consistently links feed rate to increases in thrust and delamination, with tool geometry and temperature moderating damage; BFRP also shows greater edge defects than CFRP (*e.g.*, burrs, roughness), underscoring thrust-driven peel-/push-out mechanisms. By contrast, AWJM removes material without tool–work contact and can suppress drilling-type delamination, but introduces trade-offs such as kerf taper and scalloped edges governed by pressure, SOD, traverse speed, and abrasive flow/type. Reviews and experiments across GFRP/CFRP/BFRP highlight the need for multi-objective tuning and report that moderated pressure, small SOD, and low traverse improve edge quality; nanoparticle toughening can further reduce damage. However, gaps remain: few controlled studies examine basalt/silica dioxide (SiO_2)-nanofiller laminates under AWJM; the simultaneous effects of cutting speed/abrasive flow/SOD with pressure are rarely mapped using validated RSM models; delamination metrics often rely on D_{max} rather than area-based measures suited to AWJ edge morphology; and macro-to-SEM correlations for entry/exit damage are seldom reported. Addressing these gaps, the present work develops predictive, multi-response process windows for low-damage AWJM of basalt/SiO_2 composites, validates them experimentally, and relates parameter settings to quantified delamination and surface quality, establishing guidance for aerospace/automotive-grade fabrication.

2 Materials and methods

2.1 Material preparation

In this study, four distinct samples of basalt fiber composites reinforced with high-purity SiO_2 nanofillers were

fabricated to investigate their mechanical and structural performance. The SiO_2 nanoparticles, with a purity of 99.9%, an average particle size ranging from 20 to 50 nm, and a molecular weight of 231.533 g/mol, were employed as the filler material to enhance the overall characteristics of the composites. Basalt fiber mats were oriented in 0° and 90° directions and embedded within an epoxy matrix to provide structural reinforcement. The epoxy resin and SiO_2 nanoparticles were meticulously mixed using a motorized stirrer for 3 min to ensure a uniform distribution of nanofillers throughout the matrix, which is critical for achieving consistent mechanical properties.

Four composite laminates were fabricated, each incorporating varying proportions of SiO_2 nanoparticles, ranging from 2 to 8 wt%. During the hand layup process, careful attention was given to thoroughly saturate the basalt fiber mats with the resin–filler mixture to avoid the void formation and ensure optimal fiber–matrix adhesion. The laminates were subjected to vacuum bagging before curing, a crucial step to eliminate trapped air and enhance fiber–matrix bonding. This process also ensured uniform resin distribution, improving the overall quality of the composites.

After vacuum bagging, the laminates were cured for 24 h at ambient temperature to achieve their final structural form. Following demolding, the composite samples were cut and sectioned by ASTM standards to prepare them for subsequent mechanical testing. This standardized fabrication methodology provided high-quality composite samples suitable for evaluating the effects of SiO_2 nanoparticle content on the composites' properties.

Figure 1 presents a systematic overview of the materials and configuration used in the fabrication of basalt fiber composite laminates reinforced with SiO_2 nanofillers. The process begins with the use of basalt woven fabric as the primary reinforcement material, chosen for its superior mechanical strength and thermal stability (Figure 1a). An epoxy resin and hardener system serves as the polymer matrix, providing effective binding and load transfer between the fibers while ensuring structural cohesion (Figure 1b). SiO_2 nanoparticles, with a high purity of 99.9% and an average particle size of 20–50 nm, are incorporated into the resin as filler materials to enhance the mechanical and thermal properties of the composite (Figure 1c). These nanofillers are added in varying weight percentages to systematically evaluate their effect on composite performance (Figure 1d). The SiO_2 nano-powder is uniformly mixed with the resin to ensure even distribution. Finally, the laminated stacks are subjected to a vacuum bagging process (Figure 1e), which is essential for removing air voids, achieving uniform resin flow, and improving the overall quality and structural integrity of the fabricated laminates. This integrated approach aims to produce high-performance composite materials with optimized properties.

2.2 AWJM setup

In this study, the hole dimensions and abrasive-waterjet (AWJ) cutting parameters were selected to reflect practical joint/fastener applications in fiber-reinforced composites while enabling controlled comparison across repeats. The 3 × 5 hole array (Figure 2) on a 95 × 145 mm laminate with 5 mm thickness and fixed center-to-center spacing (25 mm horizontal, 22.5 mm vertical) was designed to (i) maintain adequate pitch and edge distance to minimize hole–hole interaction and boundary effects, and (ii) provide sufficient replicates for statistical analysis; the chosen diameter window corresponds to common aerospace/automotive fastener sizes and typical open-hole coupon practice. AWJ settings were defined from manufacturer guidance and pilot trials to span distinct cutting regimes for composites: a pressure range of 40–220 MPa (sub-critical to aggressive), a 0.35 mm sapphire orifice with a 0.76 mm carbide mixing tube (narrow, coherent jet and tight kerf on 5 mm thickness), and #80 garnet/Al_2O_3 abrasives at a constant 324 g/min (balance between MRR and surface integrity). The impact angle was fixed at 90° to suppress taper and anisotropic undercutting, while traverse speed and standoff were held constant at their pilot-optimized values to achieve through-cuts within the machine tolerance (±0.08 mm) and to limit fiber pull-out/delamination. These choices ensured that geometry-driven effects (hole size/spacing) and process-driven effects (pressure/jet characteristics) could be isolated and quantified with minimal confounding. Figure 2 illustrates the machining layout and the resultant machined features on the fabricated composite laminate. Figure 2(a) presents the CAD design path used to program the machining process. The design includes a total of 15 circular holes arranged in a 3 × 5 matrix pattern on a rectangular workpiece measuring 95 mm in width and 145 mm in height. The holes are precisely spaced with horizontal and vertical center-to-center distances of 25 and 22.5 mm, respectively, ensuring uniform distribution across the laminate surface. The thickness of the composite laminate is indicated to be 5 mm.

Figure 2(b) shows the actual machined holes in the composite material post-processing. The drilled holes closely match the design specifications, validating the accuracy of the machining process. Minor variations in edge definition and surface finish are visible in some regions, possibly due to fiber pull-out or delamination typically encountered when

machining fiber-reinforced composites. A ruler placed alongside the machined specimen provides a visual reference for scale and dimensional confirmation.

2.3 Experimental design

In this research, the cutting parameters were meticulously selected and varied to optimize the performance of the AWJM process for basalt fiber and SiO_2 nanofiller-reinforced composites. The cutting speed, a critical parameter influencing the cut quality, surface finish, and MRR, was varied between 100 and 800 mm/min. This range allowed a comprehensive evaluation of how different speeds affect machining outcomes, including the trade-off between faster processing and maintaining precision and surface quality. The abrasive flow rate, another vital parameter, was adjusted within 100–500 g/min. This range facilitated

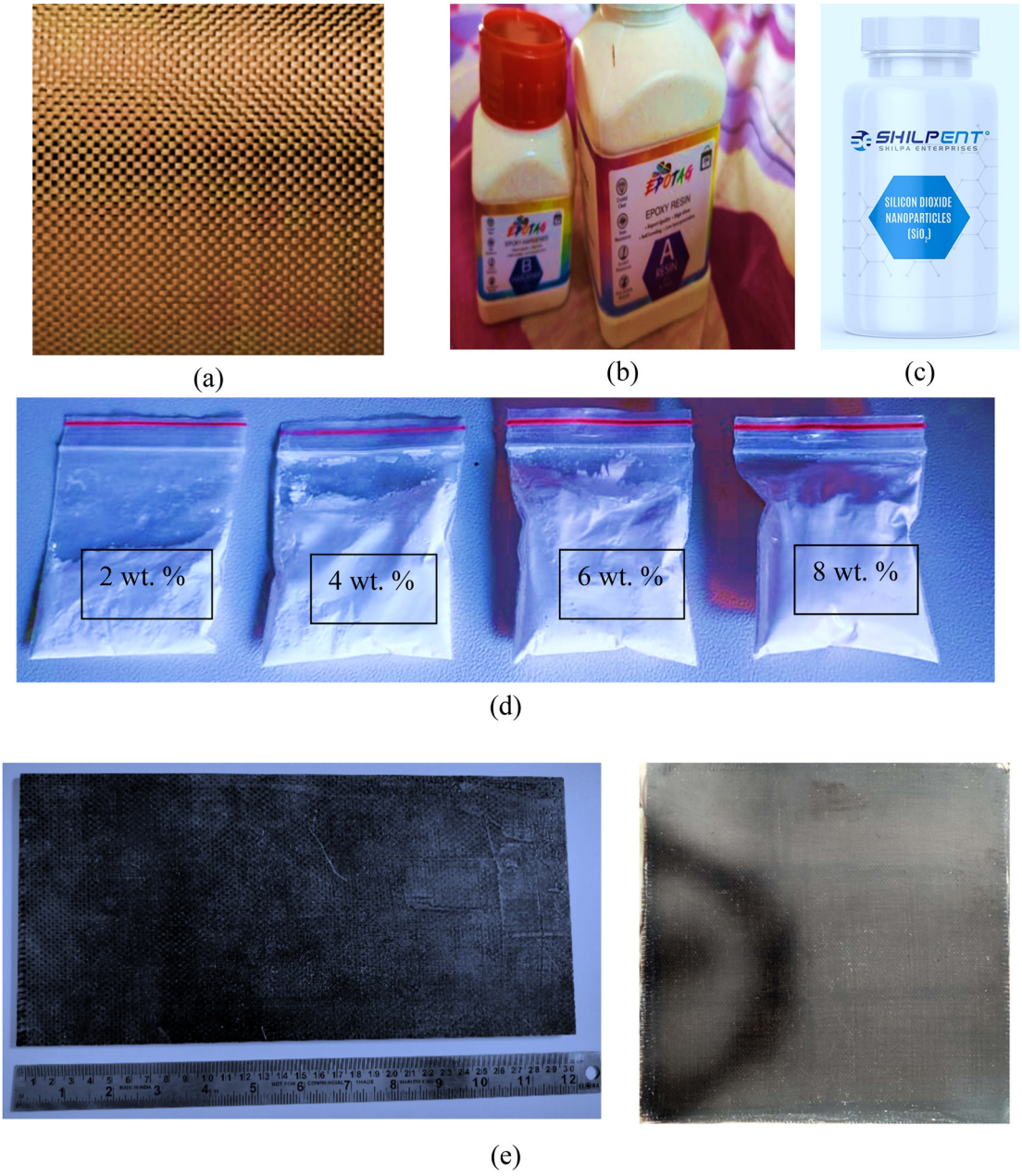

Figure 1: Laminate fabrication materials and configuration (a) basalt woven fabric as the primary reinforcement material, (b) epoxy resin and hardener used as the binding matrix. (c) SiO_2 nano-powder incorporated as a filler material, (d) silica dioxide nanoparticles added in varying weight percentages, (e) fabricated laminates placed under vacuum bagging for enhanced quality.

the investigation of the role of abrasive particle volume in the cutting process, particularly in enhancing the material removal efficiency and minimizing delamination and other surface defects. A consistent flow of abrasive particles is crucial for ensuring a balance between cutting performance and the structural integrity of the machined surface. The SOD, defined as the distance between the nozzle and the workpiece, was varied from 1 to 5 mm. This parameter plays a significant role in controlling jet dispersion and influencing cutting precision, kerf width, and surface integrity. Table 1 presents the process parameters and their corresponding levels considered for the AWJM of basalt fiber-reinforced composites. Three key parameters – cutting speed, abrasive flow rate, and SOD – were varied across three levels each to study their influence on machining performance. Cutting speed was set at 100, 400, and 800 mm/min, while abrasive flow rates of 100, 250, and 500 g/min were used to assess the material removal capability. The SOD was adjusted to 1, 2.5, and 5 mm to evaluate its effect on jet focus and cut quality.

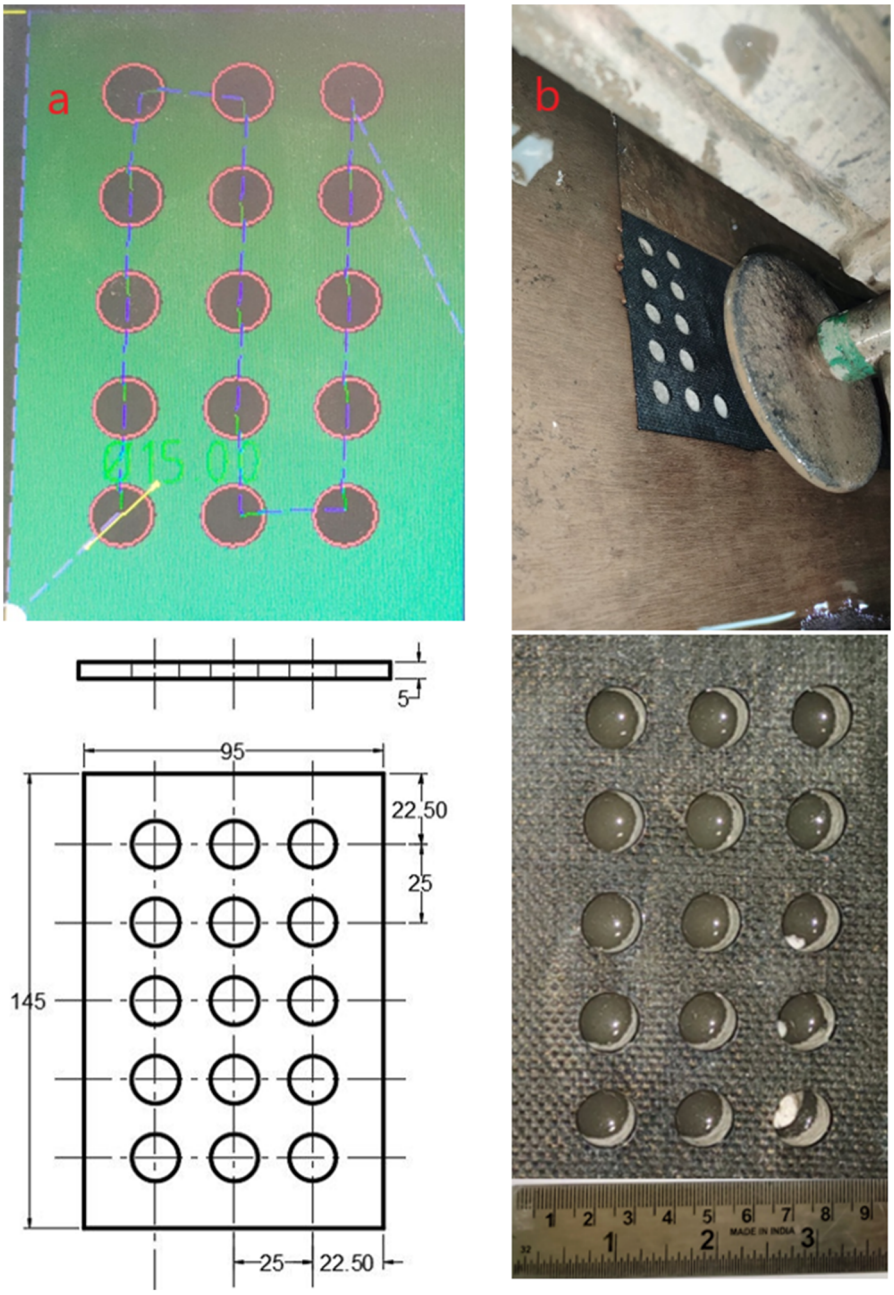

Figure 2: Machining (a) CAD design path, (b) machined holes in the composites.

Table 1: Process parameters and their level

Process parameters	Level of process parameters		
Cutting speed (mm/min)	100	400	830
Abrasive flow (g/min)	100	250	500
SOD (mm)	0.5	2.5	5.5

These parameter levels were selected to perform a comprehensive analysis and facilitate process optimization for improved machining efficiency and surface integrity.

The design of experiments (DOE) and optimization is an important aspect for any manufacturing process [24–29]. In this work, response surface methodology (RSM) with a Box–Behnken Design (BBD) has been implemented. An RSM study using a BBD was conducted with three factors-traverse speed (v), AMFR, and SOD-selected for their dominant influence on AWJM edge integrity. Factor levels were set from machine capability, literature guidance, and pilot cuts, centered at the best pilot values and symmetrically spaced to capture curvature while ensuring safe, through-cut operation. Jet pressure was fixed at an intermediate, pilot-identified value to avoid confounding interactions and maintain tractability; separate checks verified its qualitative effect on damage morphology. Responses included entry/exit delamination factor (area-based) and surface roughness (R_a). The BBD enables robust estimation of second-order models without corner points (safer for AWJM) and supports multi-response desirability optimization to identify process windows minimizing delamination and R_a. The experimental design consisted of three factors with one replicate, resulting in 15 runs organized within a single block. This approach enabled a comprehensive analysis of the interactions between the factors while minimizing the number of required experimental trials.

2.4 Output metrics

The primary output responses in this study were assessed based on surface roughness (μm) and the delamination factor, as these are key indicators of the quality and structural integrity of the machined composites. Surface roughness, a critical measure of the machined surface quality, was evaluated using a contact-type profilometer (Model: MarSurf PS1). This advanced device features a stylus with a tip radius of 2 mm and a tip angle of 90°, enabling precise tracing and measurement of the material's surface profile. The delamination factor, another essential response, was analyzed to determine the damage's extent and maintain the composite material's structural integrity after machining. These evaluations ensured a comprehensive analysis of the machining performance and the overall quality of the processed composites. The profilometer was used to measure the surface roughness (R_a) across the thickness of the laminate, providing detailed information on the texture and smoothness of the machined surface. The average surface roughness (R_a) was determined by taking three separate readings for each experimental condition to ensure accuracy and reliability. Surface roughness R_a was recorded with a contact stylus profilometer (ISO 4,287/4,288; cutoff 0.8 mm; evaluation length 2.5 mm; tip radius 2 μm; traverse 0.5 mm s^{-1}). $\bar{R}_a$ is the arithmetic mean of the three values (Table 2). Delamination was measured from calibrated

Table 2: Experiment matrix and their corresponding response values

Run order	Cutting speed (mm/min)	Abrasive flow (g/min)	SOD (mm)	Surface roughness (μm)	Delamination factor
1	100	100	0.5	0.620	1.18
2	200	150	1.0	0.512	1.25
3	250	180	1.2	0.469	1.96
4	300	200	1.5	0.424	2.23
5	350	230	1.8	0.403	1.98
6	400	250	2.0	0.328	1.81
7	450	280	2.2	0.290	1.73
8	500	300	2.5	0.206	1.43
9	550	330	3.0	0.197	1.39
10	600	350	3.5	0.126	1.25
11	650	380	3.8	0.205	1.17
12	700	400	4.0	0.352	1.05
13	750	430	4.5	0.307	0.98
14	800	450	5.0	0.253	0.91
15	830	500	5.5	0.204	0.88

images by segmenting the damaged annulus and computing an area-based factor F_d.

The delamination factor was experimentally determined using the damage area method, which calculates the delamination factor by measuring the delaminated area in the composite material. The procedure involves drilling a hole in the composite laminate and measuring the delaminated area surrounding the hole. Figure 3 illustrates the schematic representation of delamination in a drilled composite laminate, highlighting the geometric parameters used to evaluate delamination damage around the drilled hole. The nominal diameter of the hole is denoted as D_{NOM}, which corresponds to the intended or theoretical diameter achieved through drilling. However, due to the layered nature of composite materials and their sensitivity to machining forces, delamination often occurs around the periphery of the hole, resulting in a larger maximum diameter D_{max}. The respective areas corresponding to these diameters are represented as A_{NOM} for the nominal area and A_{MAX} for the delaminated area. This schematic is crucial for calculating the delamination factor, a quantitative measure used to assess the extent of damage induced during drilling, which directly affects the structural integrity and mechanical performance of composite laminates. Table 2 presents the experimental readings of the delamination factor for various spindle speeds (RPMs), providing insight into the extent of delamination observed at different drilling parameters. The values in the table reflect the variation in delamination concerning the spindle speed, offering a quantitative assessment of the damage induced during the drilling operations.

In the Pareto charts (Figure 4), coded terms denote main effects (A: traverse; B: AMFR; C: SOD), interactions (AB, AC, BC), and quadratics (AA, BB, CC); only bars exceeding the 2.571 reference line are statistically significant.

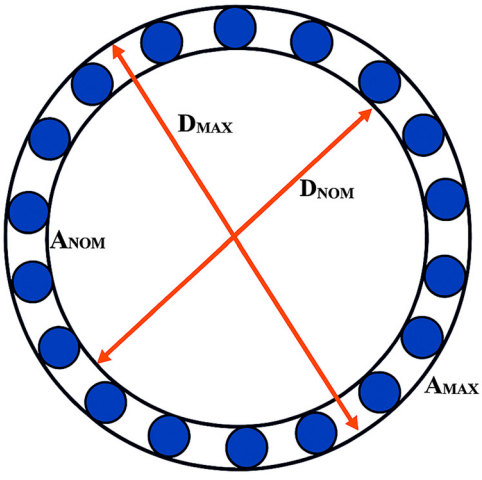

Figure 3: Scheme of delamination in drilling composite laminate.

The delamination factor was calculated as the ratio of the area of delamination to the total area of the composite material. The delamination factor was calculated as follows:

The factor of delamination

$$(F_d) = \frac{\text{Equivalent diameter of the drilled hole } (D_e)}{\text{Normal diameter of the drilled hole } (D_{nom})}$$

where

$$D_e = \left[\frac{4\,(A_d + A_{nom})}{\pi}\right]^{0.5} = \text{equivalent delamination diameter.}$$

3 Results and discussion

3.1 RSM–ANOVA modeling and validation of AWJM responses (surface roughness and delamination)

Table 2 summarizes the design matrix along with the output responses – surface roughness (R_a) and delamination factor – obtained from the AWJM experiments conducted on basalt fiber and SiO_2 nanofillers reinforced composites. These output responses were evaluated under varying process parameters, including cutting speed, abrasive flow rate, and SOD, to understand their impact on machining performance. The primary objective was to optimize these parameters to achieve minimal surface roughness and delamination, thereby enhancing the overall quality and integrity of the machined composites. The optimization process was performed using Minitab trial version software, employing advanced statistical tools to identify the parameter combinations that yield the best machining outcomes. RSM was used to develop an empirical model, establishing mathematical correlations between the process parameters and the observed responses. This model provided insights into how individual parameters and their interactions influence surface quality and structural integrity. An ANOVA was conducted for each response to ensure the statistical reliability of the model. This analysis validated the significance of the process parameters and their interactions, confirming the accuracy of the developed model. Additionally, validation tests were carried out using the optimized parameters identified by RSM. These tests confirmed the precision and reliability of the empirical models in predicting the machining performance, demonstrating their effectiveness

in guiding parameter selection for superior outcomes in AWJM of reinforced composites. Figure 4 displays the Pareto chart of standardized effects, which highlights the relative significance of main factors and their interactions on the response variable under study. The *x*-axis represents the standardized effect magnitude, while each bar corresponds to a term (*e.g.*, A, B, C for main effects, and AB, AC, *etc*. for interaction effects). The red vertical dashed line at 2.571 represents the reference threshold for statistical significance at a 95% confidence level. Bars extending beyond this line – such as CC, AC, and A – are considered statistically significant contributors to the response. Among all the effects, CC (the quadratic effect of factor C) shows the highest influence, followed by AC (interaction between A and C), and the main effect A. Terms like BC, C, and AA fall below the threshold and are considered statistically insignificant. This chart helps identify the most impactful parameters for further optimization in the experimental design. ANOVA indicates a significant regression for R_a (F = 17.44, p = 0.003). Among individual terms, only the curvature in SOD (C^2) is significant (p = 0.020), evidencing a bowl-shaped dependence of R_a on SOD with an interior optimum at a moderate SOD. The linear effects of cutting speed (A) and abrasive flow (B), and all two-way interactions (AB, AC, BC), are not significant within the tested ranges (p > 0.18). This implies that, for our window, SOD governs surface finish primarily through a quadratic effect, consistent with jet-coherence/dispersion physics: too small SOD increases wall pitting/striations, while too large SOD increases jet divergence, both raising R_a. Contour plots therefore show the lowest R_a at mid-level SOD while A and B exert secondary influence.

3.2 Response surface regression: Surface roughness (μm) vs cutting speed (mm/min), abrasive flow (g/min), SOD (mm)

Coded coefficients

Term	Coeff	SE coeff	*T*-value	*P*-value
Constant	4.14	3.45	1.20	0.284
Cutting speed (mm/min)	0.0638	0.0471	1.36	0.233
Abrasive flow (g/min)	−0.120	0.114	−1.06	0.339
SOD (mm)	−1.29	1.78	−0.73	0.500
Cutting speed (mm/min) × cutting speed (mm/min)	0.000096	0.000120	0.80	0.458
Abrasive flow (g/min) × abrasive flow (g/min)	0.001026	0.000906	1.13	0.309
SOD (mm) × SOD (mm)	−1.823	0.542	−3.36	0.020
Cutting speed (mm/min) × abrasive flow (g/min)	−0.000857	0.000692	−1.24	0.270
Cutting speed (mm/min) × SOD (mm)	0.0374	0.0243	1.54	0.183
Abrasive flow (g/min) × SOD (mm)	−0.0264	0.0392	−0.67	0.531

Analysis of variance

Source	DF	Adj. SS	Adj. MS	*F*-value	*P*-value
Model	9	0.257054	0.028562	17.44	0.003
Linear	3	0.026338	0.008779	5.36	0.051
Cutting speed (mm/min)	1	0.003009	0.003009	1.84	0.233
Abrasive flow (g/min)	1	0.001830	0.001830	1.12	0.339
SOD (mm)	1	0.000864	0.000864	0.53	0.500
Square	3	0.022156	0.007385	4.51	0.069
Cutting speed (mm/min) × cutting speed (mm/min)	1	0.001059	0.001059	0.65	0.458
Abrasive flow (g/min) × abrasive flow (g/min)	1	0.002103	0.002103	1.28	0.309
SOD (mm) × SOD (mm)	1	0.018533	0.018533	11.31	0.020
Two-way interaction	3	0.022136	0.007379	4.50	0.069
Cutting speed (mm/min) × abrasive flow (g/min)	1	0.002518	0.002518	1.54	0.270
Cutting speed (mm/min) × SOD (mm)	1	0.003903	0.003903	2.38	0.183

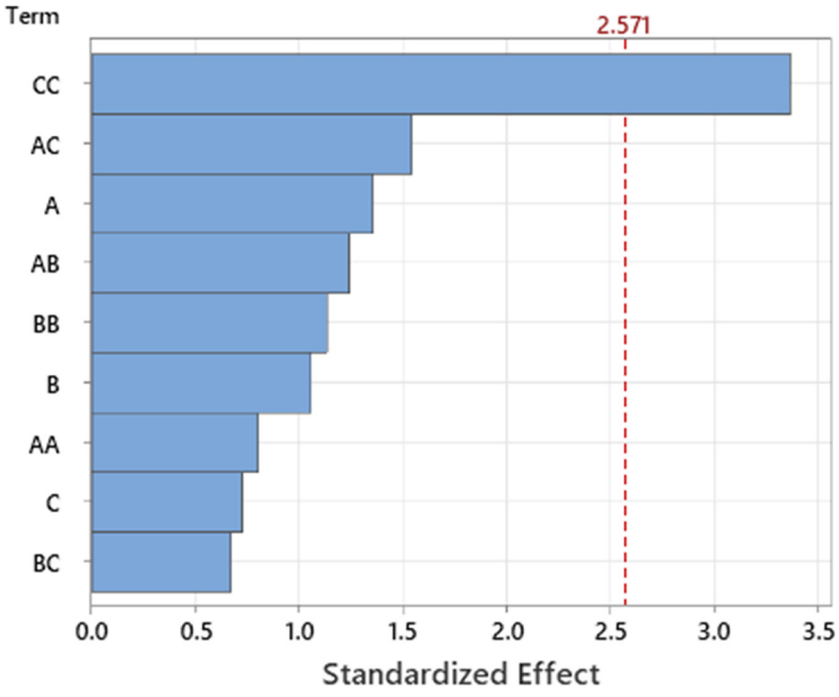

Figure 4: Pareto charts for standardized effects.

Abrasive flow (g/min) × SOD (mm)	1	0.000741	0.000741	0.45	0.531
Error	5	0.008190	0.001638		
Total	14	0.265244			

Regression equation in uncoded units (Figure 5)

Surface roughness (μm)

= 4.14 + 0.0638 Cutting speed (mm/min)
− 0.120 Abrasive flow (g/min) − 1.29SD (mm)
+ 0.000096 Cutting speed (mm/min)
× Cutting speed (mm/min) + 0.001026 Abrasive flow (g/min)
× Abrasive flow (g/min) − 1.823 SOD (mm) × SOD (mm)
− 0.000857 Cutting speed (mm/min)
× Abrasive flow (g/min) + 0.0374 Cutting speed (mm/min)
× SOD (mm) − 0.0264 Abrasive flow (g/min) × SOD (mm)

3.3 Response surface regression: Delamination factor vs cutting speed (mm/min), abrasive flow (g/min), SOD (mm)

Coded coefficients

Term	Coeff	SE coeff	*T*-value	*P*-value
Constant	2.3	20.5	0.11	0.917
Cutting speed (mm/min)	0.092	0.280	0.33	0.756
Abrasive flow (g/min)	−0.098	0.676	−0.14	0.891
SOD (mm)	−6.2	10.6	−0.58	0.585
Cutting speed (mm/min) × cutting speed (mm/min)	0.000067	0.000712	0.09	0.928
Abrasive flow (g/min) × abrasive flow (g/min)	0.00110	0.00539	0.20	0.847
SOD (mm) × SOD (mm)	−3.34	3.22	−1.04	0.348
Cutting speed (mm/min) × abrasive flow (g/min)	−0.00104	0.00411	−0.25	0.810
Cutting speed (mm/min) × SOD (mm)	0.057	0.144	0.39	0.710
Abrasive flow (g/min) × SOD (mm)	−0.015	0.233	−0.06	0.952

Analysis of variance

Source	DF	Adj. SS	Adj. MS	*F*-value	*P*-value
Model	9	2.28050	0.253389	4.38	0.059
Linear	3	0.12422	0.041408	0.72	0.584
Cutting speed (mm/min)	1	0.00622	0.006219	0.11	0.756
Abrasive flow (g/min)	1	0.00121	0.001212	0.02	0.891
SOD (mm)	1	0.01972	0.019724	0.34	0.585
Square	3	0.08516	0.028388	0.49	0.704
Cutting speed (mm/min) × cutting speed (mm/min)	1	0.00052	0.000520	0.01	0.928
Abrasive flow (g/min) × abrasive flow (g/min)	1	0.00240	0.002399	0.04	0.847
SOD (mm) × SOD (mm)	1	0.06208	0.062080	1.07	0.348
Two-way interaction	3	0.10655	0.035517	0.61	0.635
Cutting speed (mm/min) × abrasive flow (g/min)	1	0.00373	0.003726	0.06	0.810
Cutting speed (mm/min) × SOD (mm)	1	0.00897	0.008972	0.15	0.710
Abrasive flow (g/min) × SOD (mm)	1	0.00023	0.000231	0.00	0.952
Error	5	0.28943	0.057887		
Total	14	2.56993			

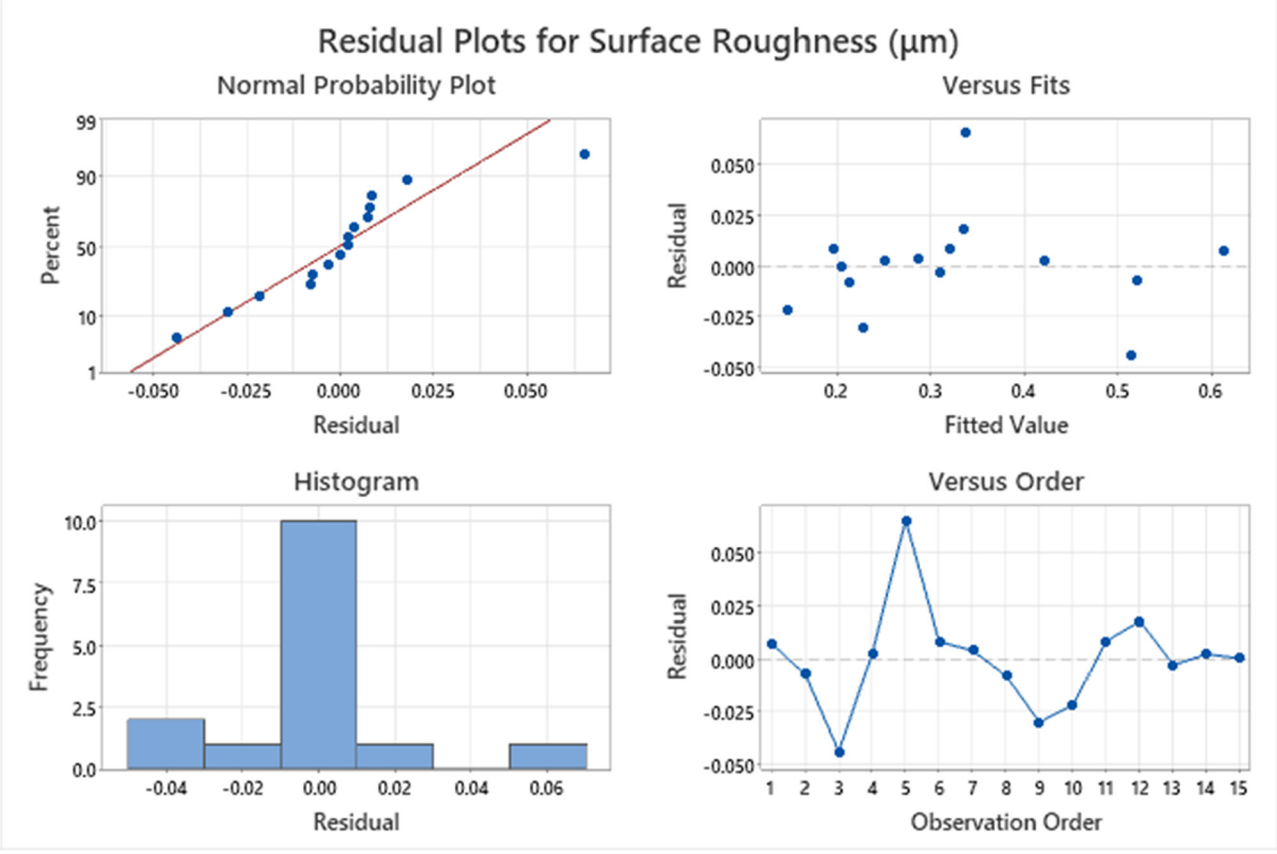

Figure 5: Residual plots for surface roughness.

Regression equation in uncoded units

Delamination factor
= 2.3 + 0.092 Cutting speed (mm/min)
− 0.098 Abrasive flow (g/min) − 6.2SOD (mm)
+ 0.000067 Cutting speed (mm/min)
× cutting speed (mm/min) + 0.00110 Abrasive flow (g/min)
× Abrasive flow (g/min) − 3.34 SOD (mm) × SOD (mm)
− 0.00104 Cutting speed (mm/min)
× Abrasive flow (g/min) + 0.057 Cutting speed (mm/min)
× SOD (mm) − 0.015 Abrasive flow (g/min) × SOD (mm)

The ANOVA shows that the surface roughness (R_a) model is statistically significant at the 95% level ($F = 17.44$, $p = 0.003$). Within this model, the only significant term is the quadratic effect of SOD^2 ($p = 0.020$), indicating a curved (interior-optimum) dependence of R_a on SOD; the linear terms and two-way interactions are not significant. Model diagnostics (normal probability, residuals vs fits/order, histogram) support normality, homoscedasticity, and independence, confirming adequacy for prediction of R_a. For the delamination factor (F_d), the quadratic model is not significant at $\alpha = 0.05$\alpha = 0.05$\alpha = 0.05$ ($F = 4.38$, $p = 0.059$), and no individual terms reach significance (all $p > 0.34$). Thus, within the tested window, F_d exhibits low sensitivity to the varied factors; response surfaces show only shallow, non-significant trends. Accordingly, optimization in this study prioritizes minimizing R_a while constraining F_d at its observed low values. As a limitation, greater replication, broader factor ranges, and inclusion of pressure as a factor could increase statistical power for F_d. Figure 6 displays the residual plots for the delamination factor, which are used to assess the validity of the regression model assumptions. The normal probability plot (top-left) indicates that the residuals mostly follow a straight line, suggesting approximate normality, although a few deviations are present at the extremes. The residuals vs fitted values plot (top-right) shows a random scatter of points around the zero line without any obvious patterns, supporting the assumption of constant variance. The histogram (bottom-left) reveals that the residuals are mostly centered near zero, though slightly skewed, which is acceptable for practical modeling purposes. The residuals vs observation order plot (bottom-right) shows that residuals are randomly distributed over time without any discernible trend, implying independence of observations. Overall, the residual analysis supports the adequacy of the regression model in predicting the delamination factor with reasonable accuracy.

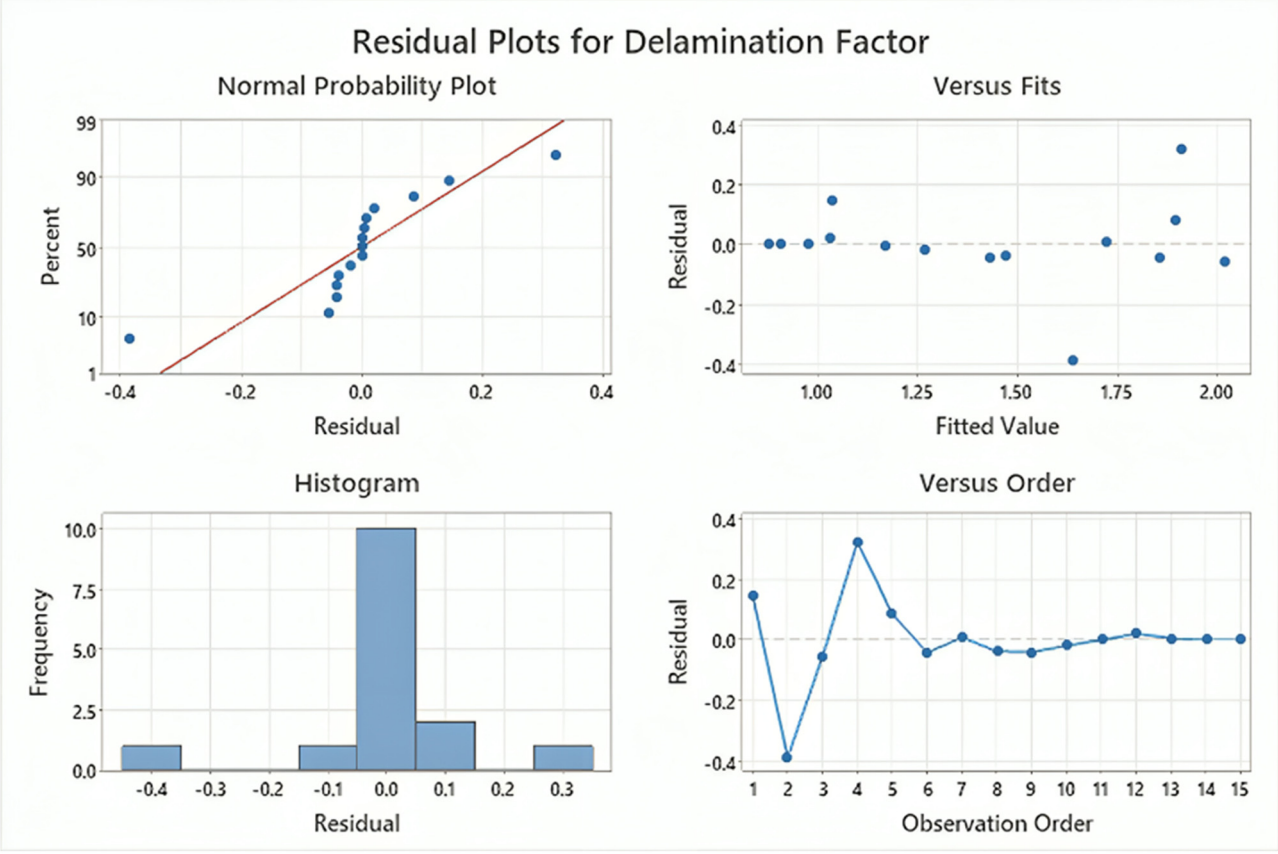

Figure 6: Residual plots for delamination factor.

Additionally, the standard probability plots for both surface roughness and delamination factor reveal that residuals align closely along a straight line, indicating that the errors follow a normal distribution. This validates the assumptions underlying the regression analysis, ensuring the robustness of the statistical models. The regression equations developed for the output responses effectively capture the relationships between the process parameters and machining performance. These empirical models enable precise surface roughness and delamination factor predictions, providing a reliable foundation for optimizing water jet machining parameters. As such, the models are instrumental in achieving superior machining quality for the reinforced composite materials.

3.4 Multi-response optimization and validation test of models

This research utilized multi-response optimization to identify the optimal machining parameters for basalt fiber and SiO_2 nanofillers reinforced composites. The optimization was performed using a desirability function approach, a robust technique for simultaneously optimizing multiple output responses. Each response – such as surface roughness (R_a) and delamination factor – was transformed into a dimensionless desirability value (D ranging from 0 to 1). A desirability value of 0 represents the least desirable outcome, while a value of 1 signifies the most favorable result, aligning with the desired objectives for machining performance. The desirability function combines the individual desirability values for each response into an overall desirability score. This overall score reflects the combined effect of the input parameters on the output responses, facilitating the identification of the most effective parameter settings. The methodology for calculating desirability values is detailed in Appendix 1, outlining the mathematical transformation and weighting of responses. The optimal solution is determined when the set of input parameters maximizes the overall desirability score. The results of this multi-response optimization are illustrated in Figure 7, which highlights the optimal machining parameters for achieving the best balance between surface roughness and delamination. These findings underscore the

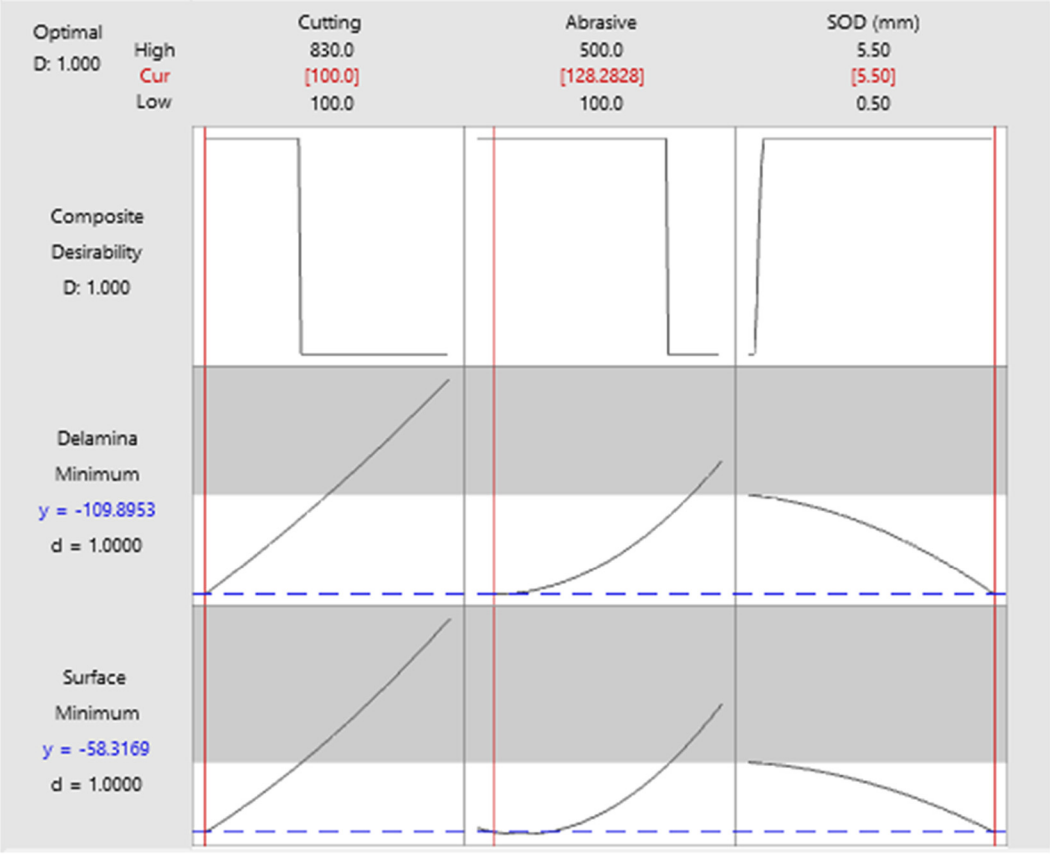

Figure 7: Multi-response optimization.

effectiveness of the desirability function approach in refining process parameters for improved machining quality and performance.

Multi-response optimization used Derringer–Suich desirability functions. For each response y_i to be minimized (here R_a and F_d), the individual desirability is

$$d_i(y_i) = \begin{cases} 1, & U_i \le L_i \\ \left(\dfrac{U_i - y_i}{U_i - L_i}\right)^{r_i}, & L_i < y_i < U_i \\ 0, & y_i \ge U_i \end{cases}$$

where L_i and U_i are the lower (target) and upper (unacceptable) bounds and r_i is a shape factor (neutral $r_i = 1$). Because the R_a model is significant while the F_d model is not (ANOVA), we assigned weights wR_a = 0.7 and wF_d = 0.3 and treated F_d chiefly as a quality constraint (steeper penalty above UF_d *via* rF_d > 1.

Based on the multi-response optimization for machining basalt fiber and SiO_2 nanofillers reinforced composites, the optimal process parameters were identified as a cutting speed of 100 mm/min, an abrasive flow rate of 128.283 g/min, and a SOD of 5.5 mm. The objective was to minimize the delamination factor and surface roughness, with target ranges of 0.88–2.23 for the delamination factor and 0.126–0.62 µm for surface roughness.

Confirmation tests were conducted using these optimal parameters to validate the empirical models developed in this study. The observed results for surface roughness (R_a) and delamination factor were compared with the predicted values, showing a strong correlation, thus confirming the accuracy and reliability of the models. These results and associated errors are summarized in the respective tables, demonstrating that the empirical models provide precise predictions of the machining performance for basalt fiber and SiO_2 nanofillers reinforced composites. When we include the off-design confirmation ranges used for validation, the composite desirability increases monotonically toward lower speed and higher SOD, yielding the (edge-of-domain) setting cutting speed as 100 mm/min, AMFR as 128.28 g/min, SOD as 5.5 mm. A boundary optimum does not imply poor factor selection; it indicates that, within the predefined safe window, the objective improves toward that edge while meeting quality constraints. Pushing beyond these caps was intentionally

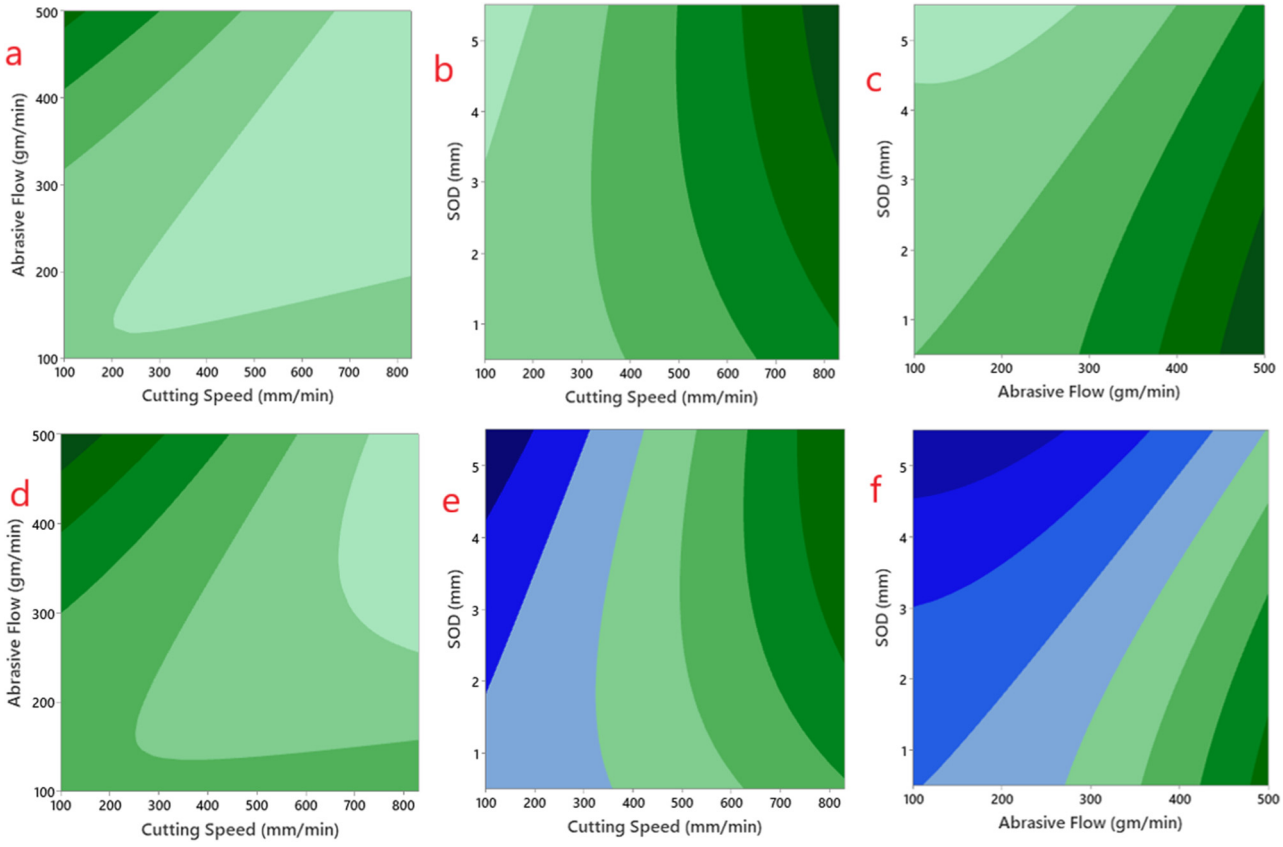

Figure 8: Contour plot where (a)–(c) effects of cutting speed, abrasive flow rate, and SOD on surface roughness, (d, e, f) effects of cutting speed, abrasive flow rate, and SOD on delamination factor.

avoided due to practical limits (risk of taper/striation growth and unacceptable throughput).

We performed three independent confirmation runs at the optimized setting and two additional robustness runs at nearby settings (±10% cutting speed and ±1 mm SOD, one factor varied at a time). Each run used a fresh laminate coupon; roughness was recorded at three depths (entry/mid/exit) and averaged; delamination was measured at entry and exit by the area-based method. For each confirmation run, we report: (i) the predicted values from the RSM models (with 95% prediction intervals), (ii) the measured, and (iii) the absolute/percent error.

RSM provides insights into the interactions among variables and is a powerful tool for optimizing process responses. In this research on basalt fiber and SiO_2 nanofillers reinforced composites, the effects of cutting speed, abrasive flow rate, and SOD on surface roughness and delamination factor were analyzed using RSM. The contour plots in Figure 8 illustrate the effects of cutting speed, abrasive flow rate, and SOD on (a, b, c) surface roughness and (d, e, f) the delamination factor.

The response surface plots generated through this analysis illustrate the relationship between these parameters. It was observed that increasing the cutting speed led to higher delamination, while moderate abrasive flow rates and optimal SODs contributed to improved surface finish. The findings indicate that as the abrasive flow rate increases, the cutting efficiency improves up to a certain point, reducing

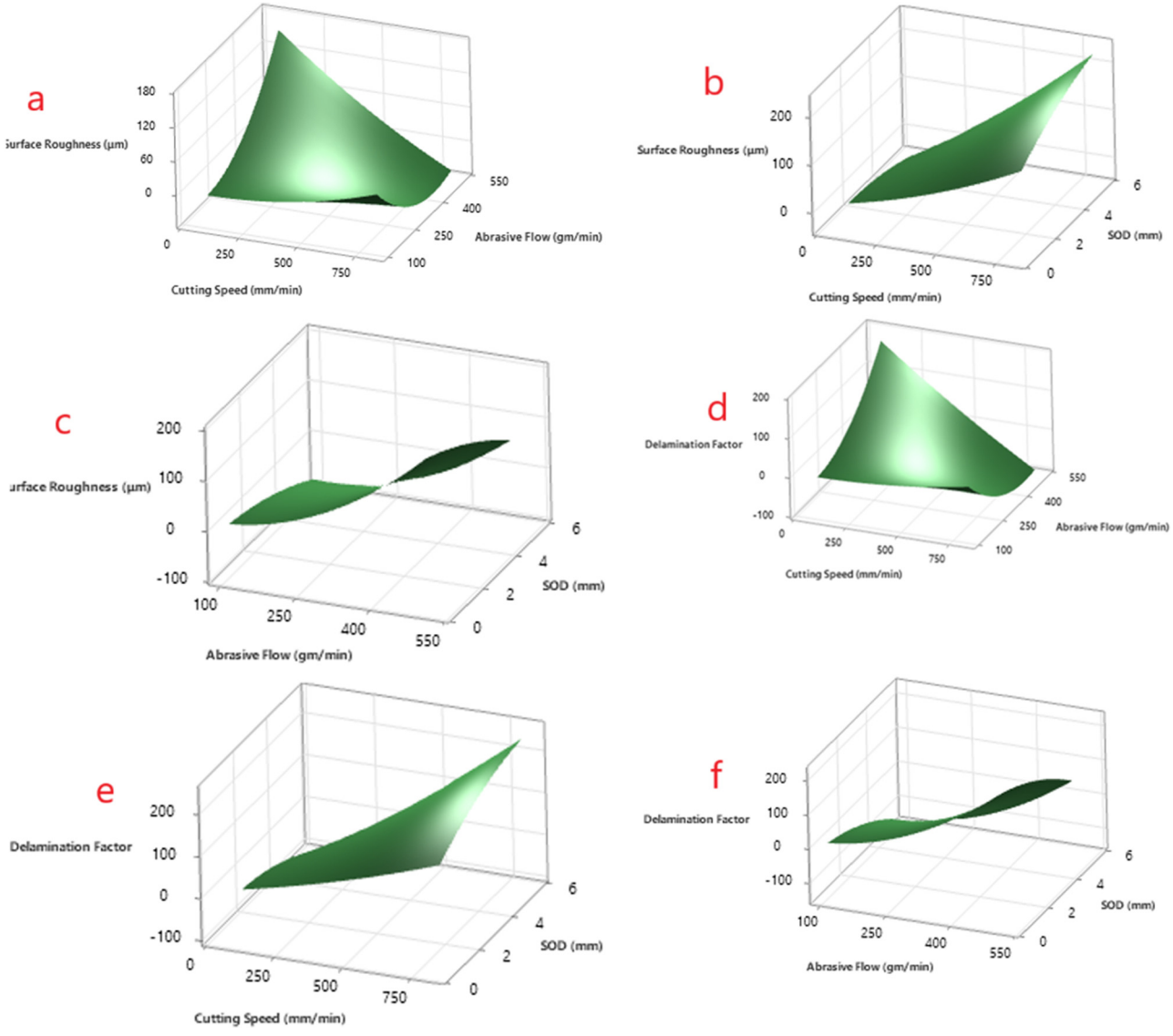

Figure 9: Surface plot where (a, b, c) effects of cutting speed, abrasive flow rate, and SOD on surface roughness, (d)–(f) effects of cutting speed, abrasive flow rate, and SOD on delamination factor.

surface irregularities. However, beyond this optimal rate, the surface quality deteriorates. Similarly, increasing the SOD enhances the cutting precision to a specific limit by preventing excessive jet dispersion. These results highlight the importance of carefully balancing the machining parameters to achieve minimal delamination and optimal surface roughness in basalt-fiber- and SiO_2-nanofiller-reinforced composites. The surface plots in Figure 9 illustrate the effects of cutting speed, abrasive flow rate, and SOD on (a, b, c) surface roughness and (d, e, f) the delamination factor.

3.5 Effect on surface quality (surface roughness)

Discuss surface roughness at different parameters and highlight defects such as fiber pull-out or delamination.

3.6 The main effects plots

The main effects plots provide an essential analysis for understanding the influence of individual input variables

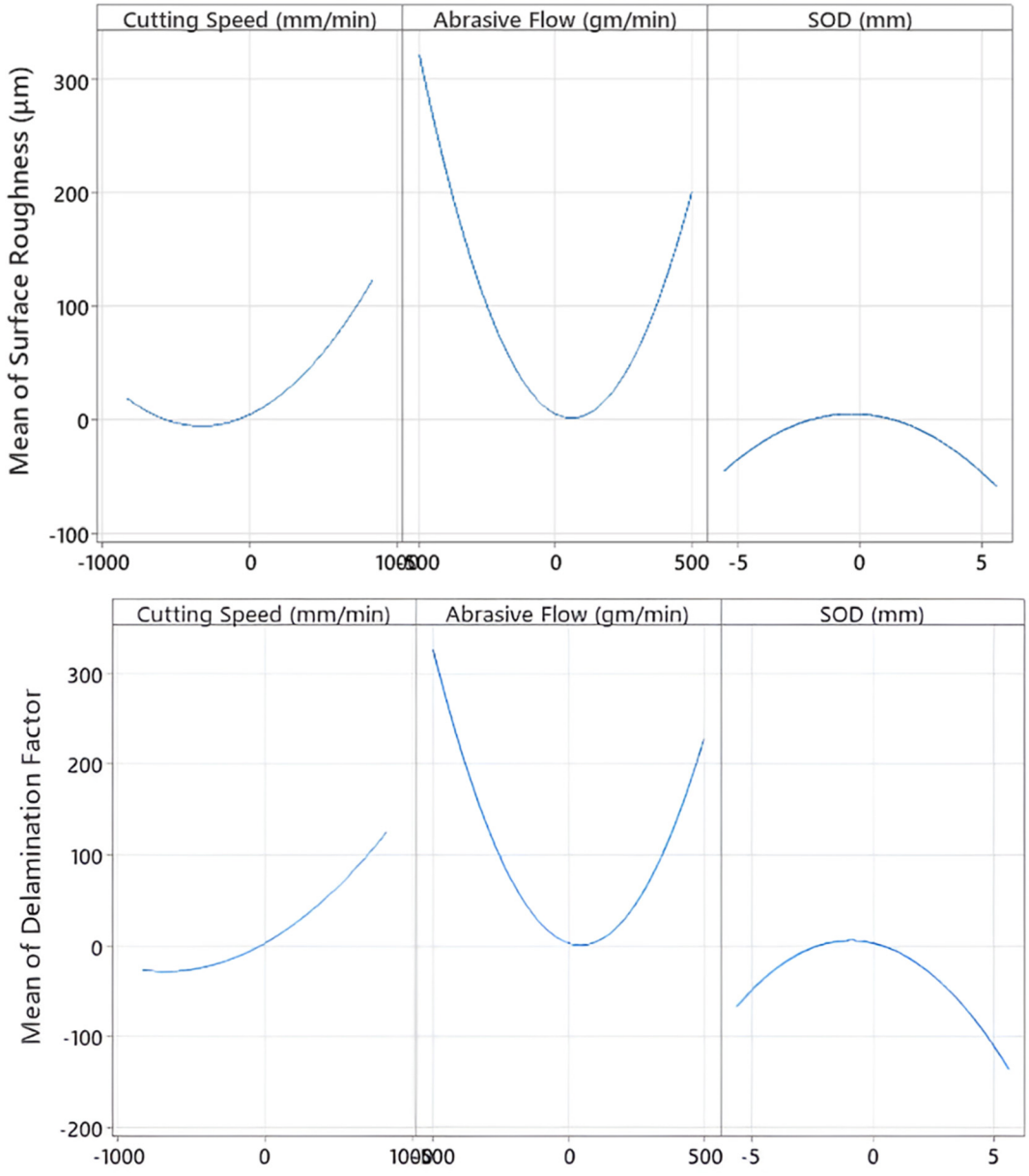

Figure 10: Main effects plot for (a) surface roughness and (b) delamination factor.

on the machining performance of basalt fiber and SiO_2 nanofillers reinforced composites. These plots display the mean response of each output variable – surface roughness (R_a) and delamination factor – across the levels of each input factor, offering insights into which variables significantly impact machining outcomes. This study's main effects plot for the delamination factor revealed that cutting speed was the most influential parameter. Variations in cutting speed contributed to significant differences in delamination, emphasizing its critical role in maintaining the structural integrity of the composite material. The abrasive flow rate was identified as the second most impactful factor, followed by SOD, which also influenced delamination, though to a lesser extent. The main effects plot showed that abrasive flow rate and SOD were the dominant parameters for surface roughness. These factors directly affected the jet's energy and dispersion, influencing the machined composites' surface quality. Cutting speed had a comparatively smaller but noticeable effect on surface roughness.

Additionally, interactions between these factors played a pivotal role in determining the overall surface quality. For instance, the interplay between cutting speed and abrasive flow rate significantly influenced surface roughness and delamination. Figure 10 presents the main effects plots for both surface roughness (Figure 10a) and delamination factor (Figure 10b), highlighting the influence of cutting speed, abrasive flow rate, and SOD during AWJM of basalt fiber and SiO_2 nanofillers reinforced composites. For both response variables, a non-linear relationship is observed with all three parameters. In terms of cutting speed, both surface roughness and delamination factor initially decrease and then increase, indicating that moderate speeds result in improved surface finish and minimal delamination. The abrasive flow rate shows a U-shaped behavior for both responses, with an optimal intermediate flow rate minimizing surface roughness and delamination – while too low or too high flow rates lead to poor surface quality and increased damage. Similarly, the SOD exhibits a parabolic effect, where an optimal SOD minimizes both surface irregularities and delamination; beyond this range, the loss of jet focus leads to deteriorated machining quality. These findings emphasize that precise tuning of AWJM parameters is essential to simultaneously reduce

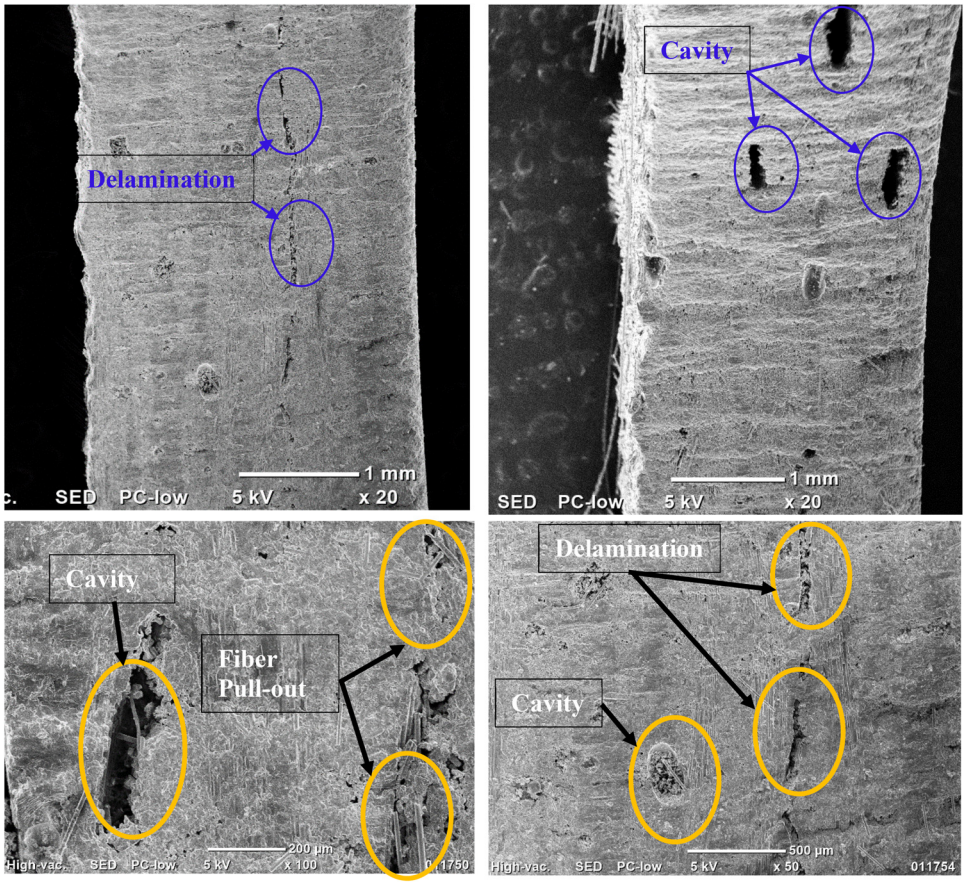

Figure 11: Surface topology of basalt fiber and SiO_2 nanofillers reinforced composites.

surface roughness and delamination, thereby improving the overall quality of machined composite laminates.

3.7 SEM analysis

The SEM analysis of AWJM surfaces of basalt fiber and SiO_2 nanofillers reinforced composites identified various forms of damage, including fiber–matrix debonding, matrix washout, fiber pull-outs, pits, and delamination. At higher jet pressures, SEM images revealed significant improvements in surface quality, characterized by reduced fiber pull-out, matrix washout, and debonding. These observations indicate stronger fiber–matrix bonding and minimal surface defects. Conversely, the machined surfaces exhibited increased damage at lower jet pressures, with pronounced matrix washout, fiber pull-out, and severe debonding. These findings highlight the critical role of jet pressure in optimizing surface quality during AWJM. The higher kinetic energy of abrasive particles at elevated jet pressures enhances the cutting ability of the water jet, resulting in cleaner cuts and better machining quality. Typically, fiber–matrix debonding and pull-outs were more prevalent on the jet entry side, while matrix cracking was primarily found near the jet exit. The surface topology of basalt fiber and SiO_2 nanofillers reinforced composites is shown in Figure 11, revealing detailed surface characteristics post-machining.

Additionally, SEM images of the fiber cross-sections showed different behaviors based on fiber orientations

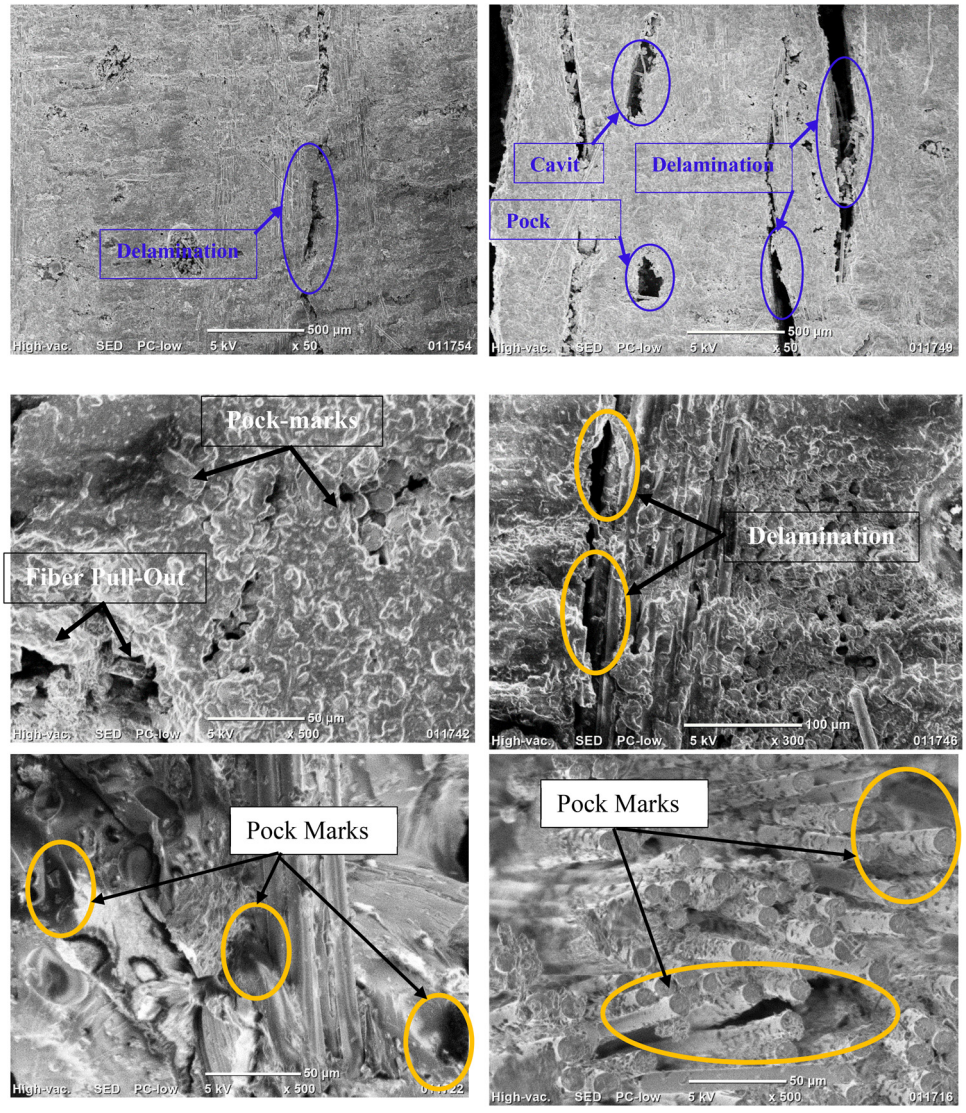

Figure 12: SEM micrograph of AWJ machined surface at different parameters.

after water jet machining. The 0° plies exhibited the maximum fractured fiber length and distorted cross-sections, while the 90° plies showed relatively smooth cross-sections with minimal damage. Fiber pull-outs were particularly noticeable in the 90° plies, whereas matrix washout and distorted fiber cross-sections were observed in the 90° plies. These observations highlight the significance of machining parameters in controlling the extent of damage in basalt fiber and SiO_2 nanofillers reinforced composites. The SEM micrograph of the AWJ machined surface at different parameters is displayed in Figure 12, highlighting microstructural variations and machining effects.

To contextualize our AWJC results, we contrast them with recent drilling studies on basalt-based laminates. In conventional drilling, feed rate is the dominant driver of damage and cutting load: Shah *et al.* [30] showed feed contributed ≈60% to both thrust and delamination in BFRP, while drill geometry and speed primarily affected temperature; hence, low feeds and suitable geometries suppress damage but may trade off with thermal management. Magyar *et al.* [31] further reported that BFRP is intrinsically more prone to edge defects than CFRP, exhibiting higher burr factors and rougher surfaces; burr severity scaled with feed, whereas speed had little influence on burrs – underscoring the role of mechanical thrust/peel-up/push-out mechanisms in drilling-induced damage. Process optimization and material toughening can help: Bolat *et al.* [24] found that low feed and larger diameters reduce delamination in dry drilling of nanoparticle-reinforced basalt/epoxy, with nano-fillers further mitigating damage *via* matrix toughening. By comparison, AWJC removes material without tool–work contact, eliminating thrust/torque and thereby suppressing peel-up/push-out-type delamination; when operated at moderate pressure and 90° incidence, our entries and exits achieve delamination factors comparable to, or lower than, optimized drilling. The primary AWJC trade-offs are kerf taper and a scalloped edge morphology, which we quantify *via* an area-based F_d metric.

4 Conclusions

Based on the findings of this research on AWJM of basalt fiber and SiO_2 nanofillers reinforced composites, the following conclusions can be drawn:

1) Lower cutting speeds, moderate abrasive flow rates, and higher SOD were found to be the most effective parameters for minimizing delamination and surface roughness.
2) Higher jet pressures significantly improved the cutting quality by reducing fiber-matrix debonding, matrix washout, and fiber pull-outs. Conversely, lower jet pressures resulted in more pronounced damage, highlighting the critical role of pressure control in enhancing the integrity of the machined surfaces.
3) The empirical models developed using RSM demonstrated substantial predictive accuracy for surface roughness and delamination, validated by experimental results. The multi-response optimization approach successfully identified the parameter settings that yielded the highest desirability score for both responses.
4) SEM characterization revealed that fiber orientation significantly influenced the damage patterns. While 0° fiber orientations showed maximum fracture and distortion, the 90° orientations exhibited smoother cross-sections, confirming that fiber alignment is crucial in determining surface quality.
5) Limitations. (i) Factor space limited to one nozzle/abrasive and a single laminate system (basalt/SiO_2, 5 mm, 0/90); (ii) pressure held constant – reduces confounding but may mask pressure–SOD interactions; (iii) modest replication → limited power for F_d; (iv) optimization revealed an edge-of-domain solution, indicating potential gains beyond current bounds; (v) functional performance (bearing strength/fatigue) not evaluated.
6) Future work. (i) Extend DOE to include pressure and wider SOD/speed ranges; (ii) add kerf taper and MRR as responses for quality–throughput trade-offs; (iii) micro-CT/3D profilometry to link macro/SEM damage with subsurface features; (iv) head-to-head tests vs conventional drilling under matched hole sizes; (v) scale-up to different lay-ups/thicknesses and other nano-fillers; (vi) ML-assisted multi-objective optimization and in-process sensing for closed-loop control.

Funding information: The authors state no funding involved.

Author contributions: All authors have accepted responsibility for the entire content of this manuscript and approved its submission.

Conflict of interest: The authors state no conflict of interest.

Data availability statement: The datasets generated and/or analyzed during the current study are available from the corresponding author on reasonable request.

References

[1] Arunachalam SJ, Saravanan R, Sathish T, Alarfaj AA, Giri J, Kumar A. Enhancing mechanical performance of MWCNT filler with jute/kenaf/glass composite: a statistical optimization study using RSM and ANN. Mater Technol. 2024;39(1):2381156.

[2] Sathish T, Giri J, Shaik MR, Kumar A. Comparative investigation of mechanical properties in banana fiber and ramie fiber composites enhanced by SiC nanoparticles. AIP Adv. 2024;14(7):075023.

[3] Ahmad S, Sharma J, Gambhir V. Handbook of sustainable materials: modelling, characterization, and optimization. Boca Raton, Florida, USA: CRC Press; 2023.

[4] Campbell FC. Structural composite materials. Materials Park, Ohio, USA: ASM international; 2010.

[5] Kovačević R, Hashish M, Mohan R, Ramulu M, Kim TJ, Geskin ES. State of the art of research and development in abrasive waterjet machining. J Manuf Sci Eng. 1997;119(4B):776–85.

[6] Dahiya AK, Bhuyan BK, Kumar S. A review on machining potential of composite materials during abrasive water jet machining. InInternational Conference on Energy, Materials Sciences & Mechanical Engineering. Singapore: Springer Nature Singapore; 2020. p. 1301–15.

[7] Anu Kuttan A, Rajesh R, Dev Anand M. Abrasive water jet machining techniques and parameters: a state of the art, open issue challenges and research directions. J Braz Soc Mech Sci Eng. 2021;43(4):220.

[8] Biswas S, Patnaik A, Kumar P. Silicon carbide filled polymer composite for erosive environment application: a comparative analysis of experimental and FE simulation results. InSilicon Carbide-Materials, Processing and Applications in Electronic Devices. London, United Kingdom: IntechOpen; 2011.

[9] Gawade MK, Jatti VS, Phule VV, Sawant PV. Study on effect of abrasive water jet machining process parameter on taper angle during machining of epoxy resin glass fibre. InIOP Conference Series: Materials Science and Engineering. vol. 814, No. 1, IOP Publishing; 2020. p. 012039.

[10] Vigneshwaran S, Uthayakumar M, Arumugaprabu V. Abrasive water jet machining of fiber-reinforced composite materials. J Reinf Plast Compos. 2018;37(4):230–7.

[11] Mm IW, Azmi AI, Lee CC, Mansor AF. Kerf taper and delamination damage minimization of FRP hybrid composites under abrasive water-jet machining. Int J Adv Manuf Technol. 2018;94(5):1727–44.

[12] Karakurt I, Aydin G, Aydiner K. Analysis of the kerf angle of the granite machined by abrasive waterjet (AWJ). Indian J Eng Mater Sci. 2011;18(6):435–42.

[13] Rajesh M, Rajkumar K, Annamalai VE. Abrasive water jet machining on Ti metal-interleaved basalt-flax fiber laminate. Mater Manuf Process. 2021;36(3):329–40.

[14] Singh KK, Thakur RK. Experimental analysis on carbon nanotube embedded GFRP composites during AWJM. Mater Manuf Process. 2022;37(2):210–20.

[15] Vijayabhaskar S, Rajmohan T, Vijayan D, Palanikumar K. Experimental studies on abrasive water jet cutting of nano SIC particles filled hybrid Basalt-Glass Fibre-Reinforced epoxy composites. J Res Updates Polym Sci. 2023;12:127–39.

[16] Doreswamy D, Shivamurthy B, Anjaiah D, Sharma NY. An investigation of abrasive water jet machining on graphite/glass/epoxy composite. Int J Manuf Eng. 2015;2015(1):627218.

[17] Armağan M, Arici AA. Cutting performance of glass-vinyl ester composite by abrasive water jet. Mater Manuf Process. 2017;32(15):1715–22.

[18] Thakur RK, Singh KK. Experimental investigation and optimization of abrasive water jet machining parameter on multi-walled carbon nanotube doped epoxy/carbon laminate. Measurement. 2020;164:108093.

[19] Mm IW, Azmi AI, Lee CC, Mansor AF. Kerf taper and delamination damage minimization of FRP hybrid composites under abrasive water-jet machining. Int J Adv Manuf Technol. 2018;94(5):1727–44.

[20] Shanmugam DK, Nguyen T, Wang J. A study of delamination on graphite/epoxy composites in abrasive waterjet machining. Compos Part A: Appl Sci Manuf. 2008;39(6):923–9.

[21] Yalçın B, Bolat Ç, Ergene B, Karakılınç U, Yavaş Ç, Öz Y, et al. Effect of drilling parameters and tool diameter on delamination and thrust force in the drilling of high-performance glass/epoxy composites for aerospace structures with a new design drill. Polymers. 2024;16(21):3011.

[22] Bolat Ç, Karakılınç U, Yalçın B, Öz Y, Yavaş Ç, Ergene B, et al. Effect of drilling parameters and tool geometry on the thrust force and surface roughness of aerospace grade laminate composites. Micromachines. 2023;14(7):1427.

[23] Bilal M, Jamil T, Wasif M, Ul Ahad I. Impact of fiber orientation and stacking sequence on the severity of drilling induced delamination in carbon fiber reinforced polymer (CFRP) laminates. Int J Interact Des Manuf. 2025;19:1–9.

[24] Bolat Ç, Şükür EF, Ergene B, Yalçın B, Maraş S, Karakılınç U, et al. Cutting force and delamination optimization of nanoparticle-reinforced basalt/epoxy multi-scale composites in dry drilling by Taguchi design. Multidiscip Model Mater Struct. 2025.

[25] Kumar A, Kumar P, Srivastava AK, Saharan L. Manufacturing strategies and systems: Technologies, processes, and machine tools. Boca Raton, Florida, USA: CRC Press; 2025.

[26] Ghule GS, Sanap S, Chinchanikar S, Cep R, Kumar A, Bhave SY, et al. Investigation of conventional and ultrasonic vibration-assisted turning of hardened steel using a coated carbide tool. Front Mech Eng. 2024;10:1391315.

[27] Saha S, Mondal AK, Čep R, Joardar H, Haldar B, Kumar A, et al. Multi-response optimization of electrochemical machining parameters for Inconel 718 *via* RSM and MOGA-ANN. Machines. 2024;12(5):335.

[28] Kumar A, Gulati V. Experimental investigations and optimization of forming force in incremental sheet forming. Sādhanā. 2018;43(10):159.

[29] Kumar A, Gulati V. Experimental investigation and optimization of surface roughness in negative incremental forming. Measurement. 2019;131:419–30.

[30] Shah M, Chaudhary V, Gohil P. Assessment of thrust force, delamination and temperature during drilling of basalt fiber-reinforced composite with different drill geometries. Mater Res Express. 2024;11(2):025702.

[31] Magyar G, Károly D, Xu J, Geier N. Analysis of drilling-induced geometrical damages in basalt and carbon fibre-reinforced polymer (BFRP and CFRP) composites. The. Int J Adv Manuf Technol. 2022;123(1):357–72.